

Kinase Activity Profiling of Gram-Negative Pneumonia

Arie J Hoogendijk,^{1,2} Sander H Diks,⁴ Maikel P Peppelenbosch,⁵ Tom van der Poll,^{1,2} and Catharina W Wieland^{1,3}

¹Center for Infection and Immunity Amsterdam, ²Center for Experimental and Molecular Medicine, and ³Laboratory of Experimental Intensive Care and Anesthesiology, Academic Medical Center, Amsterdam, the Netherlands, ⁴Department of Cell Biology, Section Immunology, University Medical Center Groningen, University of Groningen, Groningen, the Netherlands, and ⁵Department of Gastroenterology and Hepatology, Erasmus Medical Center, Rotterdam, the Netherlands

Pneumonia is a severe disease with high morbidity and mortality. A major causative pathogen is the Gram-negative bacterium *Klebsiella (K.) pneumoniae*. Kinases play an integral role in the transduction of intracellular signaling cascades and regulate a diverse array of biological processes essential to immune cells. The current study explored signal transduction events during murine Gram-negative pneumonia using a systems biology approach. Kinase activity arrays enable the analysis of 1,024 consensus sequences of protein kinase substrates. Using a kinase activity array on whole lung lysates, cellular kinase activities were determined in a mouse model of *K. pneumoniae* pneumonia. Notable kinase activities also were validated with phospho-specific Western blots. On the basis of the profiling data, mitogen-activated protein kinase (MAPK) signaling via p42 mitogen-activated protein kinase (p42) and p38 mitogen-activated protein kinase (p38) and transforming growth factor β (TGF β) activity were reduced during infection, whereas v-src sarcoma (Schmidt-Ruppin A-2) viral oncogene homolog (avian) (SRC) activity generally was enhanced. AKT signaling was represented in both metabolic and inflammatory (mitogen-activated protein kinase kinase 2 (MKK), apoptosis signal-regulating kinase/mitogen-activated protein kinase kinase kinase 5 (ASK) and v-raf murine sarcoma viral oncogene homolog B1 (β -RAF)) context. This study reaffirms the importance of classic inflammation pathways, such as MAPK and TGF β signaling and reveals less known involvement of glycogen synthase kinase 3 β (GSK-3 β), AKT and SRC signaling cassettes in pneumonia.

© 2011 The Feinstein Institute for Medical Research, www.feinsteininstitute.org

Online address: <http://www.molmed.org>

doi: 10.2119/molmed.2011.00011

INTRODUCTION

Pneumonia is a severe disease associated with high morbidity and mortality (1). In the United States, nearly 100,000 deaths are attributed to pneumonia and sepsis per year, making these the fifth leading causes of death (2). The Gram-negative bacterium *Klebsiella (K.) pneumoniae* is a common causative pathogen in pneumonia (3–5).

The innate immune system provides the first immunological interface between the host and invading pathogens. Pattern recognition receptors (PRRs) expressed by immune cells can detect conserved motifs present in microorganisms termed pathogen-associated

molecular patterns (PAMPs), thereby initiating an inflammatory response designed to eliminate the intruder (6). In Gram-negative pneumonia, Toll-like receptors (TLRs) recognize several PAMPs, including lipopolysaccharide (LPS) (TLR4), DNA (TLR9), RNA (TLR3), Porins/peptidoglycan (TLR2) and flagellin (TLR5) (7,8). NOD-like receptors (NLRs) may interact with DNA (AIM2) (9), peptidoglycan (NOD2, NALP1/3) and flagellin (IPAF) (9,10). Multiple PRRs detect their respective PAMPs simultaneously and interplay between pathways is highly likely to arise during an evolving infection (7,11).

Reversible phosphorylation, mediated by protein kinases and phosphatases, regulates signal transduction pathways (12). The outcome of these phospho-transfer activities is beyond the simple linear signal transduction models. A broader perspective of this complex system is enabled by array techniques. Kinome profiling represents a method to obtain activity data of kinases and their respective pathways (13). Here, we utilized a kinase activity array with 1,024 consensus sequences to reveal sequential processes during the course of *K. pneumoniae* pneumonia in mice. We identified and validated activity patterns of classic immune-related kinases, such as p38 mitogen-activated protein kinase (p38) and p42 mitogen-activated protein kinase (p42), as well as other key regulators of cellular responses such as glycogen synthase kinase 3 β (GSK-3 β) and the v-src sarcoma (Schmidt-Ruppin A-2) viral oncogene

Address correspondence and reprint requests to AJ Hoogendijk, Meibergdreef 9, G2-105, 1105 AZ Amsterdam, the Netherlands. Phone: +31-20-5666034; Fax: +31-20-6977192; Email: a.j.hoogendijk@amc.uva.nl.

Submitted January 7, 2011; Accepted for publication March 9, 2011; Epub (www.molmed.org) ahead of print March 15, 2011.

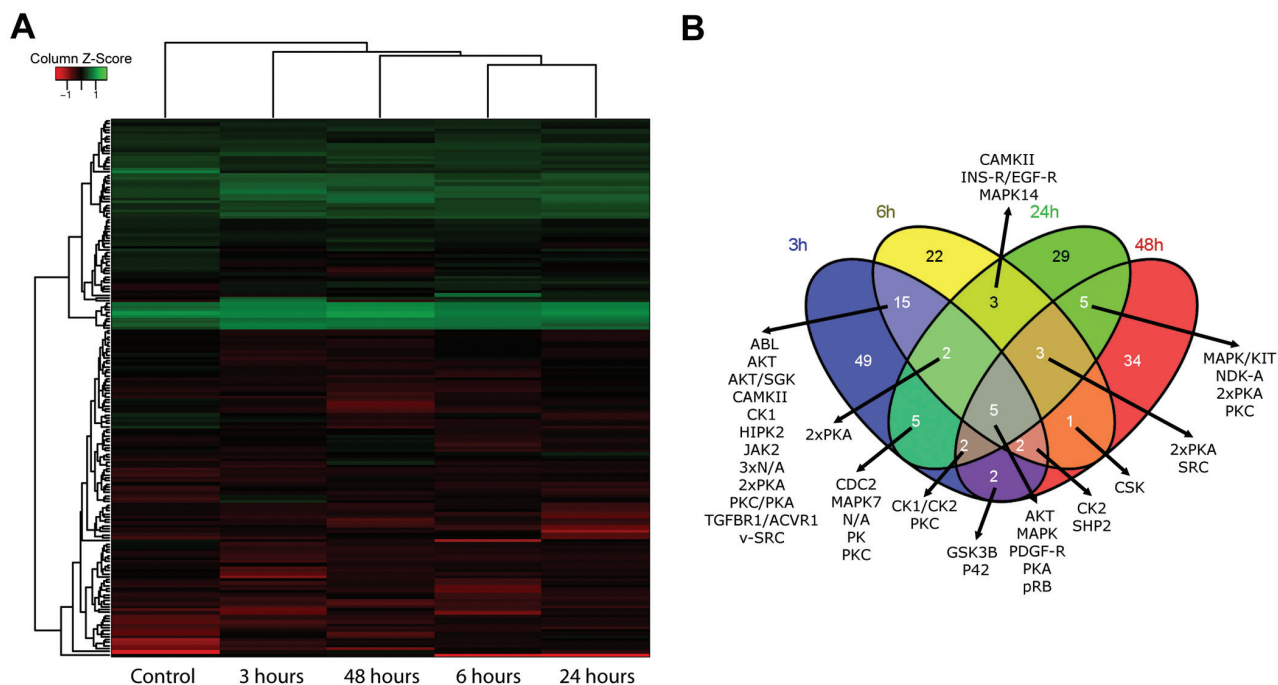


Figure 1. Heat map and clustering of phosphorylation states of 179 significantly altered kinase activities in whole lung lysates (A). Note that the distance between the cluster of infection and control is the greatest. Venn diagram (B) depicting the distribution of phosphorylated spots at time points indicated; 3 h is depicted in blue, 6 h in yellow, 24 h in green and 48 h in red. Most data points are confined to their respective time points. pRB, retinoblastoma kinase; N/A, not available (this spot has no consensus upstream kinase).

homolog (avian) (SRC) and AKT cassettes.

MATERIAL AND METHODS

Animals

Female C57Bl6 mice (aged 10 wks) were purchased from Charles River (Maas-tricht, the Netherlands). The Animal Care and Use Committee of the University of Amsterdam approved all experiments.

Induction of Pneumonia/Inflammation

Bacterial pneumonia was induced as described previously (11,14). *K. pneumoniae* serotype 2 (ATCC 43816) were grown in Tryptic Soy broth (Difco, Detroit, MI, USA) to midlogarithmic phase at 37°C. Bacterial cultures were harvested by centrifugation at 2,900g for 15 min, washed twice and resuspended in sterile saline at a concentration of 10⁴ CFU/50 µl. Mice were inoculated with 50 µl of bacterial suspensions intranasally under isoflurane (Upjohn, Ede, the Netherlands) inhalation anes-

thesia. Control mice were intranasally inoculated with sterile saline.

Determination of Bacterial Load

At 3, 6, 24 and 48 h after infection, three mice were euthanized by cardiac puncture under Domitor (Pfizer Animal Health Care, Capelle aan den IJssel, the Netherlands; active ingredient medetomidine) and Nimatek (Eurovet Animal Health, Bladel, the Netherlands; active ingredient ketamine) anesthesia. Three control mice were euthanized 3 h after inoculation with sterile saline. Left lungs were harvested and homogenized in four volumes of sterile saline with a tissue homogenizer (ProScience, Oxford, CT, USA). Colony forming units (CFUs) were determined from serial dilutions of samples, plated on blood agar plates and incubated at 37°C for 16 h before colonies were counted.

Kinome Profiling

Right lungs were snap frozen in liquid nitrogen, after which they were homogenized in three volumes of lysis

buffer (MPER; Pierce, Rockville, WI, USA) supplemented with 1 mmol/L MgCl₂, 1 mmol/L glycerophosphate, 1 mmol/L Na₃VO₄, 1 mmol/L NaF, 1 µg/mL leupeptin, 1 µg/mL aprotinin and 1 mmol/L phenylmethylsulphonyl fluoride. Homogenates were centrifuged at 2,080g for 5 min and pellets were discarded. Samples were pooled and diluted to a protein concentration of 1 mg/mL. Of these lysates, 80 µL were mixed with 12 µL of Activation mix (70 mmol/L MgCl₂, 70 mmol/L MnCl₂, 400 µg/mL PEG 8000 and 47 µCi [³³P-γ]ATP) and applied to the array (Pepscan Presto, Lelystad, the Netherlands). The arrays chips were incubated at 37°C for 2 h and were washed twice in 2 mol/L NaCl (1% TWEEN 20), once in PBS (1% SDS) and rinsed twice in demineralized H₂O. After air drying, the chips were exposed to a phosphor imager plate for 72 h. [³³P-γ]ATP signals were measured with a phosphor imager (Storm, Amersham Biosciences, Uppsala, Sweden).

Analysis

Spot densities and individual backgrounds were analyzed using Scanalyze (<http://rana.lbl.gov/EisenSoftware.htm>). Data were exported to a spreadsheet for further analysis. The raw data were normalized to the 90th percentile, as described previously (15–18). From this data, the heat map in Figure 1 was constructed in R 2.12.0 (R Foundation for Statistical Computing, Vienna, Austria) using the heatmap.2 function of the gplots library, making use of the hclust function set using complete-linkage. Significance was assessed by Student *t* test on normalized data. Shared event distribution was visualized using Venny (JC Oliveros [2007] VENNY <http://bioinfo.gp.cnb.csic.es/tools/venny/index.html>).

Western Blots

Results from the kinome analysis were validated by performing phospho-specific Western blots for major kinases. Blots were done for pp38–mitogen-activated protein kinase (pp38-MAPK), pp42/44-MAPK, pSMAD1/5/8, pSRC and pGSK-3 β (Cell Signaling Technology, Boston, MA, USA) and β -actin (Santa Cruz Biotechnology, Santa Cruz, CA, USA). Samples for Western blotting were boiled at 95°C for 5 min in Laemmli buffer and loaded onto SDS-PAGE gels. After electrophoresis, the content of the gels was transferred onto Immobilon-PVDF membranes (Millipore, Billerica, MA, USA). Membranes were blocked in 5% bovine serum albumin (BSA) (Roche, Basel, Switzerland) in Tris buffered saline Tween (TBS-T) at room temperature for 60 min. All antibodies were diluted 1:500 with exception of β -actin, which was diluted 1:4000, and incubated overnight at 4°C. Next, the membranes were incubated for 60 min with antirabbit-horseradish peroxidase (HRP)–conjugated secondary antibody (Cell Signaling Technology) and blots were imaged using LumiLight Plus ECL (Roche) on a LAS 3000 chemiluminescence imager (Fujifilm, Tokyo, Japan).

Table 1. Bacterial loads and cytokine and chemokine levels in lung homogenates.^{a,b}

	3 h	6 h	24 h	48 h
CFU/lung	$4.6 \times 10^3 \pm 2.6 \times 10^3$	$9.1 \times 10^3 \pm 2.7 \times 10^3$	$3.1 \times 10^4 \pm 8.1 \times 10^3$	$3.5 \times 10^6 \pm 1.2 \times 10^6$
TNF- α (pg/mL)	501 \pm 230	402 \pm 110	905 \pm 302	1,658 \pm 904
IL-1 β (pg/mL)	79 \pm 54	84 \pm 36	414 \pm 210	484 \pm 66
IL-6 (pg/mL)	159 \pm 69	174 \pm 45	510 \pm 136	1,920 \pm 1,631
KC (pg/mL)	1,885 \pm 460	2,809 \pm 972	9,451 \pm 2,614	28,202 \pm 781
MIP-2 (pg/mL)	3,325 \pm 887	3,237 \pm 659	5,459 \pm 1,186	9,397 \pm 4,807

^aAfter inoculation of 10^4 CFU of *K. pneumoniae*, both bacterial loads and cytokine and chemokine levels increase with time.

^bData are mean \pm SD of three mice per time point.

Cytokine and Chemokine Assays

For cytokine and chemokine measurements, left lungs were excised, weighed and homogenized in four volumes of saline. Homogenates were diluted 1:2 in lysis buffer (300 mmol/L NaCl, 30 mmol/L Tris, 2 mmol/L MgCl₂, 2 mmol/L CaCl₂, 2 % Triton X-100, AEBSEF[4-(2-aminoethyl)benzeensulfonyl fluoride], EDTA-Na₂, 8 μ g/mL pepstatin and leupeptin, pH7.4) and incubated on ice for 30 min. Homogenates were centrifuged at 2,350g at 4°C for 10 min and stored at –20°C until use. Interleukin (IL)-1 β , IL-6, tumor necrosis factor- α (TNF- α), cytokine-induced neutrophil chemoattractant (KC) and macrophage inflammatory protein (MIP)-2 were measured in lung homogenates using enzyme-linked immunosorbent assays (ELISAs) (R&D Systems, Minneapolis, MN, USA) according to the manufacturer's instructions. Detection limits were: TNF- α , 62.5 pg/mL; MIP-2 and KC, 15 pg/mL; IL-1 β and IL-6: 31.25 pg/mL.

RESULTS

Induction of Pneumonia

Mice inoculated with 10^4 CFU *K. pneumoniae* developed pneumonia. Table 1 represents the bacterial loads in whole lung homogenates during the course of the experiment. Both CFU counts and cytokine/chemokine levels increased rapidly in time. Notably, this infectious dose results in approximately 80% lethality, starting from 48 h after infection (11,14). Hence, this model represents severe pneumonia, and samples were ob-

tained from shortly after infection until shortly before the first deaths occurred.

K. pneumoniae Pneumonia Kinome Profile

From the phosphorylation events of the array, a heat map was constructed (Figure 1A). The clustering of the significant events on the array chip showed that the kinase activity profiles of infected lungs were more similar to each other than those of the uninfected control animals. The highest similarity was between samples obtained after 6 and 24 h. When compared with control arrays, a total of 179 phosphorylated spots from arrays derived from infected lungs were statistically significantly different. For the 3, 6, 24 and 48 h time points, the spots were distributed as 82, 53, 54 and 54 differentially phosphorylated spots, respectively (Figure 1B). The majority of events, however, were exclusive to a single time point.

Provisional signaling cascade schemes were created from notable phosphorylated spots of the kinomics chips reflecting kinase activity during progressive Gram-negative pneumonia (Figure 2). AKT was present in the context of a number of signaling cascades (Figure 2A). AKT is a substrate to pyruvate dehydrogenase kinase (PDK) (19) (spot 934) and via GSK-3 β (spots 84, 443 and 1020) (20) and tuberlin (spot 373) signals toward mammalian target of rapamycin (mTOR) (21). Moreover, AKT is involved in the apparent downregulation of activity of kinases critical in the immune response setting; via v-raf murine sarcoma viral oncogene homolog B1 (b-RAF)

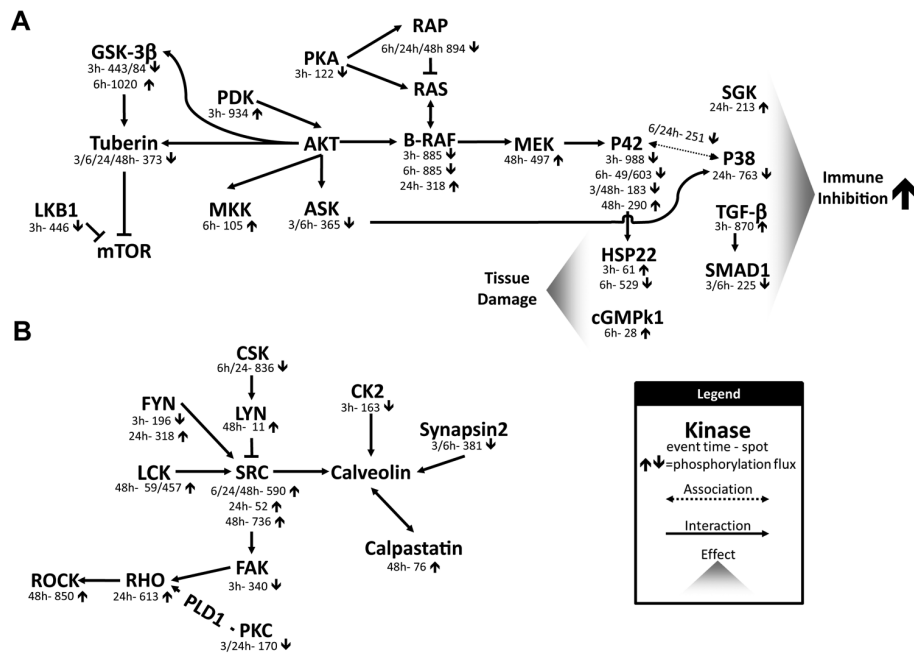


Figure 2. Provisional signaling cascades activated during the course of Gram-negative pneumonia. Immunological processes defined by p42 and p38 MAPKs, TGFβ and SRC kinase signaling are induced by pneumonia. HSP22 and cGMPk1 hint toward the occurrence of tissue damage. Also AKT and PKA axis signaling are present during *K. pneumoniae* pneumonia. PLD1, phospholipase D1.

(spots 318, 885) (22) and mitogen-activated protein kinase kinase 2 (MEK) (spot 497) (23) the activity of p42 MAPK (spots 49, 183, 290 and 988) was inhibited overall. Inhibition of p38 MAPK (spots 261 and 603) could be due to AKT-dependent modulation of apoptosis signal-regulating kinase/mitogen-activated protein kinase 5 (ASK) (spot 365) (24). The activity patterns of serum/glucocorticoid regulated kinase (SGK) (spot 213) and transforming growth factor β (TGFβ) (spot 870) are in agreement with lowered immune responses (25,26). Downstream of TGFβ, SMAD1 (27) activity was diminished after 3 and 6 h of infection.

Heat shock 22kDa protein 8 (HSP22) (spots 61 and 529) and cyclic guanosine monophosphate kinase 1 (cGMPk1) (spot 28) are representative of tissue damage, arising as a consequence of uncontrolled infection (28–30). Phosphorylation of these substrates was enhanced very early in infection, although HSP22 phosphorylation (increased 3 h after infection) was reduced significantly at 6 h of infection.

Figure 2B depicts signaling events centered by SRC (spots 52, 590 and 736). The SRC kinases protooncogene tyrosine-protein kinase Fyn (FYN) (spots 196 and 318) and leukocyte-specific protein tyrosine kinase (LCK) (spots 59 and 457) display enhanced activity after 24 and 48 h respectively (17,31,32). SRC-inhibiting kinase c-src tyrosine kinase (CSK) (spot 836) (33) activity was diminished after 6 and 24 h, intermediate between CSK and SRC, v-yes-1 Yamaguchi sarcoma viral-related oncogene homolog (LYN) (spot 11) (34) activity was enhanced after 48 h. These signals toward SRC balance out and result in overall activation of SRC kinase.

RHO signaling (spots 613 and 850), which is connected to SRC signaling also was activated (35). This activation most likely occurs via focal adhesion kinase (FAK) (spot 340) and protein kinase C (PKC) (spot 170) (36,37).

Validation of Kinome Profile Events

GSK-3β activity was present in the context of AKT signaling, and shown in

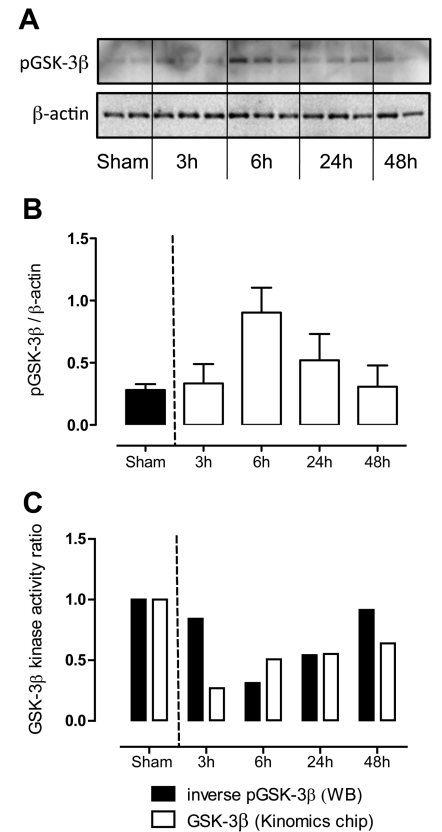


Figure 3. Validation of GSK-3β kinomics array signals. Western blots, performed for SER-9 phosphorylated GSK-3β (A and B). Phosphorylation of serine 9 results in GSK-3β deactivation. To compare Western blot data with kinase activity data, time point/sham ratios for both data sets were determined. Owing to the inhibitory outcome of the Western blot phosphorylation data, ratios of this set were inverted. Inverted Western blot ratios were compared with the time point/sham ratios of the kinase activity data from the kinomics array (C). These activity patterns overlap, showing consistency between Western blot and kinase activity array methods. Data are mean ± SD of three mice per time point.

the provisional signaling scheme signaling toward mTOR (see Figure 2A). To overlay the phosphorylation pattern of the Western blot and the activity pattern of the kinome profile, both data sets were normalized to the control. As phosphorylation of GSK-3β (Figure 3A, B) at serine 9 results in inactivation of this kinase (38), normalized Western blot data

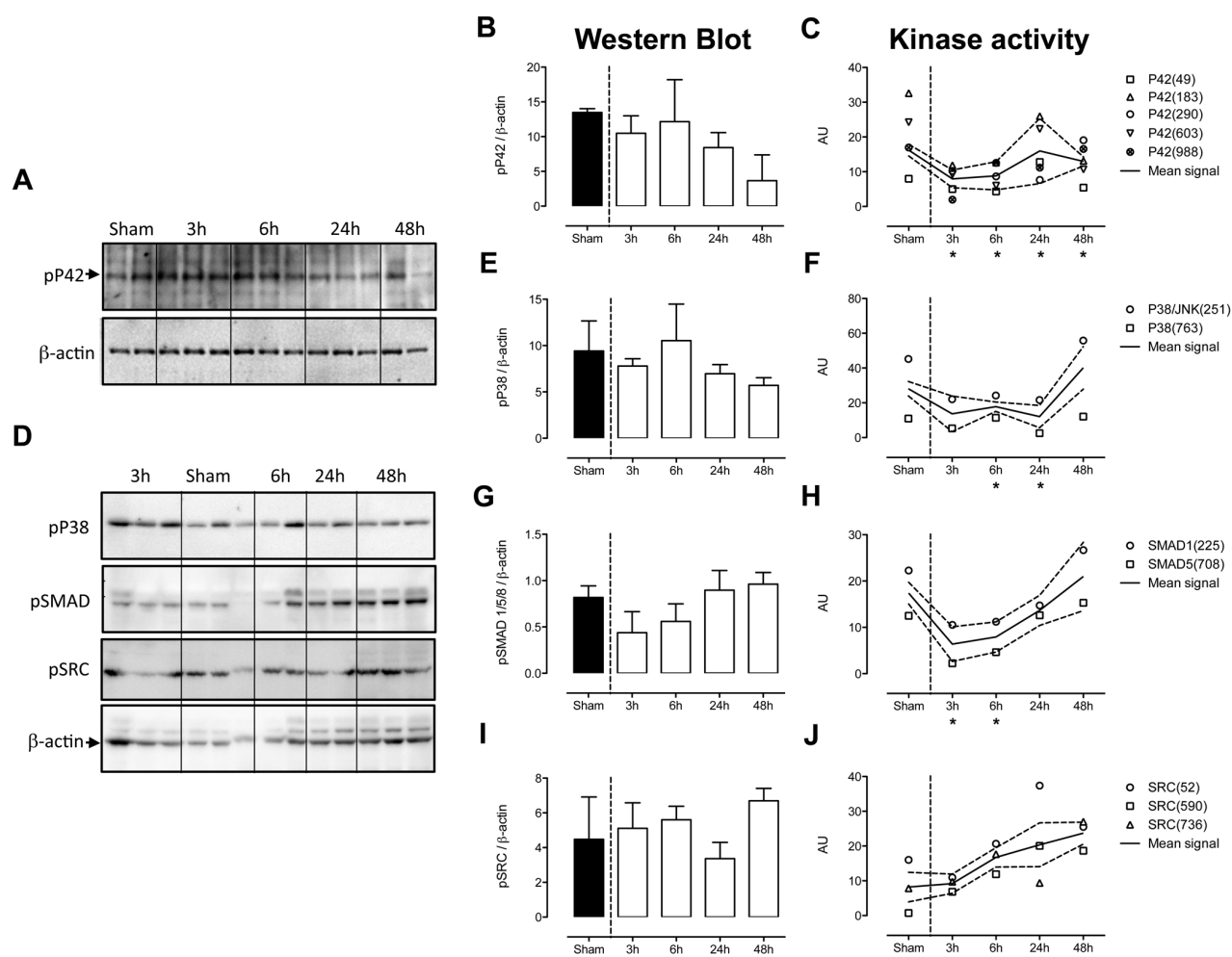


Figure 4. Validation of notable signals in the kinomics array. Western blots and quantifications were performed to validate notable signals in the kinomics chip. Western blots are shown in A and D; panels B, E, G and I contain graphs of densitometric assessment of Western blots. Kinase activity data are represented in graphs C, F, H and J. Phosphorylation patterns of p42 (A, B), p38 (D, E), SMAD1/5/8 (D, G) and SRC (D, I) based on Western blots match the kinase activity array data (C, F, H and J respectively). Array data are presented as a mean signal of two spots belonging to the kinase of interest. Asterisks indicate significant events in kinomics profile. Data are mean \pm SD of three mice per time point.

were inverted. The graph (Figure 3C) derived from the Western blot and kinome profiles showed similar activity patterns validating our array findings.

As depicted in the provisional signaling scheme, AKT is involved in down-regulation of kinases critical in the immune response setting, including P42 and P38 (22–24). Phosphorylation states of p38 and p42 kinases were compared with chip signals. p42 phosphorylation levels (Figure 4A, B) decreased over time, which is in accordance with the determined kinase activity (Figure 4C). p38

blot revealed a reduction in phosphorylation levels of p38 with the exception of the 6 h time point (Figure 4D, E).

In the kinome profile array, we found that SMAD1 activity was reduced in the early phase of infection (see Figure 2A). In addition, spot 708 phosphorylation demonstrated a similar, though not significant pattern for SMAD5 (data not shown). The phospho-specific Western blot (Figure 4D, G) matched the outcome of the kinase activity array (Figure 4H).

SRC is the heart of the provisional cascades depicted in Figure 2B. Under influ-

ence of FYN, LCK and CSK-LYN, the overall activity was increased over time on the kinomics chip (Figure 4J). With the exception of the 24 h time point, Western blot analysis revealed increasing phosphorylation of SRC during *K. pneumoniae* pneumonia (Figure 4D, I).

DISCUSSION

Genomics array data banks are becoming increasingly available to the broad public to monitor responses or predict outcomes of specific patient subgroups. However, most of these data banks con-

tain gene expression data, thus lacking information on real-time protein activities such as phosphorylation interactions which are fundamental to signaling cascades. With 1,024 consensus substrates, kinome profiling enables the direct determination of kinase activity. We report here for the first time sequential alterations in kinase activities in whole lungs during the course of severe Gram-negative pneumonia.

The inherent complexity of arrays demands a careful approach of determining activity patterns of a multitude of kinase-substrate interactions prior to drawing conclusions on individual kinase activities. The Western blots performed for pp38, pp42, pSMAD1/5/8, pSRC and pGSK-3 β resulted in activity patterns similar to those of the kinome profile, validating the data obtained from the kinomics chip.

Differences between kinase activities found between the kinomics chip and phosphorylation states determined by Western blot can be explained by differences in active kinase domains from the kinomics assay and epitopes recognized by the p-antibodies used in our validation Western blots.

In the kinome profile, pSMAD1 was reduced in the early phase of infection and enhanced at 48 hours after infection. This hints to differential activity of the TGF β receptor 1 or the BMP receptor type 1B, the kinases responsible for phosphorylation of SMAD1 at this site. BMP signaling in the lung is shown to facilitate tissue remodeling and repair and has been implicated as a cause of pulmonary hypertension (39,40).

Remodeling signals could be a response to activity of the tissue damage associated kinases HSP22 and cGMPk1 (see Figure 2A). However, under control of TGF β , SMAD1 immunological effects are in accordance with reduced p38 and p42 activities (see Figure 2A and Figure 4A–F) (39).

AKT (or PKB) regulates various cellular processes, such as survival, growth, proliferation, glucose uptake, metabolism and angiogenesis (20). It also was described as regulating TLR-dependent inflammatory responses in bone marrow

derived mouse neutrophils (19). On the kinomics array, AKT activity resulted in reduced ASK activation, thus linking this “general organizer” to inflammatory MAPK signaling. PKA influences various biologic systems. In the context of MAPK signaling, PKA has dual effects on p42 activation. When signaling via RAF-1, PKA mediates inhibition of p42, while PKA signaling via b-RAF results in activation of p42 (23). The PKA-b-RAF cascade found in our kinomics arrays is in agreement with the observed p42 kinase events.

The p38 and p42 activities were reduced during the infection, although inflammatory effectors (cytokines and chemokines) were increased. The p38 and p42 MAPK activation is transient (41,42). The activation dynamics of p38 and p42 could be such that the peak of their activation has passed already at the three-hour time point, which is in accordance with studies in human endotoxemia studies: after an early peak of activation for both p38 and p42, a reduced phosphorylation state occurred (43). To investigate the full activity dynamics of p38 and p42, in future studies, kinome analysis on earlier time points should be performed.

GSK-3 β regulates multiple cellular functions, including cell structure, and gene expression, mobility and apoptosis; additionally, GSK-3 β also is an important positive regulator of inflammatory processes (44). Inhibition of GSK-3 β reduced IL-12p40, IL-6 and TNF- α cytokine levels in mice infected with *Francisella tularensis* (45). Furthermore, TLR-induced proinflammatory cytokine production was reduced in monocytes by inhibiting GSK-3 β (44). The effects on host response by GSK-3 β are attributed to regulation of transcription factors as NF- κ B, NFAT and STATs (46). In our data (see Figure 2) GSK-3 β activity is reduced at the three-hour time point and enhanced at the six-hour time point. This is in accordance with the observed enhanced activity of TGF β , which has a known antiinflammatory effect (26) at three hours, and the reductions in p38 and p42 activity (see Figure 2).

Knowledge of the expression of SRC tyrosine kinase family members during in-

fection is limited. In accordance with our current data, enhanced SRC activity was noted in a mouse model of LPS-induced acute lung injury (47). Moreover, the SRC family inhibitor PP1 blocked LPS-induced NF- κ B activation in lung tissue via downregulation of the phosphorylation and degradation of I κ B- α at 4 or 24 hours (36); moreover, SRC family inhibition attenuated LPS-induced acute lung injury (48) supposedly via an effect on TLR signaling (49). Also, CSK mutant (CSK-GEcre) mice, which lack a general inhibitor of SRC, develop acute multifocal inflammation in skin and lung and are hypersensitive to LPS-induced shock due to unconstrained SRC activity (33). These findings support the notion that the SRC-related signals that arise from kinase activity profiling are a direct response to ongoing infection.

Pneumonia triggers a complex host response at the primary site of infection that encompasses a protective innate immune response aiming to kill invading pathogens, counterregulatory actions seeking to limit collateral tissue damage and repair processes. Kinases are important components of the integrated cellular responses during pneumonia. The current investigation is the first to provide insight in pulmonary activity of key kinases during various stages of severe Gram-negative respiratory tract infection.

Kinase activity assays enable a direct assessment of the dynamics of kinases with a higher throughput than any currently available antibody-based method. Moreover, kinase activity arrays measure the activity of kinases on their respective substrates, rather than providing indirect information on their activity via their phosphorylation state. Nonhypothesis driven experiments, made possible by an array approach, may facilitate observations outside of ruling paradigms.

Our results point to induction of innate immunity, as reflected by classic p42 and p38 MAPKs, TGF β , the lesser-known immunological side of SRC kinases, and the increasingly appreciated role of GSK-3 β in the host response. In addition, processes controlled by general organizers such as AKT and PKA were induced, of which

the exact effects are more difficult to pinpoint. This study suggests a role for SRC kinase in pneumonia and delineates a potential link of AKT and PKA with inflammatory responses. As such, kinase activity profiling may reveal new functional and pathogenetic mechanisms at play during various stages of pneumonia.

ACKNOWLEDGMENTS

We thank Joost Daalhuisen and Marieke ten Brink for their expert technical assistance.

DISCLOSURE

The authors declare that they have no competing interests as defined by *Molecular Medicine*, or other interests that might be perceived to influence the results and discussion reported in this paper.

REFERENCES

- Torres A, Rello J. (2010) Update in community-acquired and nosocomial pneumonia 2009. *Am. J. Respir. Crit. Care Med.* 181:782–7.
- Anderson RN, Smith BL. (2005) Deaths: leading causes for 2002. *Natl. Vital Stat. Rep.* 53:1–89.
- Jover F, et al. (2008) A comparative study of bacteremic and non-bacteremic pneumococcal pneumonia. *Eur. J. Intern. Med.* 19:15–21.
- Craven DE, Steger KA. (1995) Epidemiology of nosocomial pneumonia. *Chest.* 108:15–16S.
- Lin YT, Jeng YY, Chen TL, Fung CP. (2010) Bacteremic community-acquired pneumonia due to *Klebsiella pneumoniae*: clinical and microbiological characteristics in Taiwan, 2001–2008. *BMC Infect. Dis.* 10:307.
- Kawai T, Akira S. (2010) The role of pattern-recognition receptors in innate immunity: update on Toll-like receptors. *Nat. Immunol.* 11:373–84.
- Takeuchi O, Akira S. (2010) Pattern recognition receptors and inflammation. *Cell.* 140:805–20.
- Akira S, Takeda K. (2004) Toll-like receptor signalling. *Nat. Rev. Immunol.* 4:499–511.
- Rathinam VAK, et al. (2010) The AIM2 inflammasome is essential for host defense against cytosolic bacteria and DNA viruses. *Nat. Immunol.* 11:395–402.
- Mogensen TH. (2009) Pathogen recognition and inflammatory signaling in innate immune defenses. *Clin. Microbiol. Rev.* 22:240–73.
- Wieland CW, van Lieshout MHP, Hoogendijk AJ, van der Poll T. (2010) Host defense during *Klebsiella pneumoniae* relies on hematopoietic expressed TLR4 and TLR2. *Eur. Respir. J.* 37:848–57.
- Manning G, Whyte DB, Martinez R, Hunter T, Sudarsanam S. (2002) The protein kinase complement of the human genome. *Science.* 298:1912–34.
- Parikh K, Peppelenbosch MP. (2010) Kinome profiling of clinical cancer specimens. *Cancer Res.* 70:2575–8.
- Renckens R, et al. (2007) Plasminogen activator inhibitor type 1 is protective during severe Gram-negative pneumonia. *Blood.* 109:1593–601.
- Lowenberg M, et al. (2006) Kinome analysis reveals nongenomic glucocorticoid receptor-dependent inhibition of insulin signaling. *Endocrinology.* 147:3555–62.
- van Baal JWPM, et al. (2006) Comparison of kinome profiles of Barrett's esophagus with normal squamous esophagus and normal gastric cardia. *Cancer Res.* 66:11605–12.
- Parikh K, Poppema S, Peppelenbosch MP, Visser L. (2009) Extracellular ligation-dependent CD45RB enzymatic activity negatively regulates lipid raft signal transduction. *Blood.* 113:594–603.
- Diks SH, et al. (2007) Evidence for a minimal eukaryotic phosphoproteome? *PLoS ONE.* 2:e777.
- Strassheim D, et al. (2004) Phosphoinositide 3-kinase and Akt occupy central roles in inflammatory responses of Toll-like receptor 2-stimulated neutrophils. *J. Immunol.* 172:5727–33.
- Manning BD, Cantley LC. (2007) AKT/PKB signaling: navigating downstream. *Cell.* 129:1261–74.
- Cai SL, et al. (2006) Activity of TSC2 is inhibited by AKT-mediated phosphorylation and membrane partitioning. *J. Cell Biol.* 173:279–89.
- McCubrey JA, et al. (2007) Roles of the Raf/MEK/ERK pathway in cell growth, malignant transformation and drug resistance. *Biochim. Biophys. Acta.* 1773:1263–84.
- Gerits N, Kostenko S, Shiryayev A, Johannessen M, Moens U. (2008) Relations between the mitogen-activated protein kinase and the cAMP-dependent protein kinase pathways: comradeship and hostility. *Cell. Signal.* 20:1592–607.
- Kim AH, Khursigara G, Sun X, Franke TF, Chao MV. (2001) Akt phosphorylates and negatively regulates apoptosis signal-regulating kinase 1. *Mol. Cell. Biol.* 21:893–901.
- Webster MK, Goya L, Ge Y, Maiyar AC, Firestone GL. (1993) Characterization of sgk, a novel member of the serine/threonine protein kinase gene family which is transcriptionally induced by glucocorticoids and serum. *Mol. Cell. Biol.* 13:2031–40.
- Taylor AW. (2009) Review of the activation of TGF-beta in immunity. *J. Leukoc. Biol.* 85:29–33.
- Alarcón C, et al. (2009) Nuclear CDKs drive Smad transcriptional activation and turnover in BMP and TGF-beta pathways. *Cell.* 139:757–69.
- Yew EHJ, et al. (2005) Proteasome inhibition by lactacystin in primary neuronal cells induces both potentially neuroprotective and pro-apoptotic transcriptional responses: a microarray analysis. *J. Neurochem.* 94:943–56.
- Morrow G, Samson M, Michaud S, Tanguay RM. (2004) Overexpression of the small mitochondrial Hsp22 extends *Drosophila* life span and increases resistance to oxidative stress. *FASEB J.* 18:598–9.
- Zhang G, et al. (2009) Lipopolysaccharide stimulates platelet secretion and potentiates platelet aggregation via TLR4/MyD88 and the cGMP-dependent protein kinase pathway. *J. Immunol.* 182:7997–8004.
- Filipp D, et al. (2003) Regulation of Fyn through translocation of activated Lck into lipid rafts. *J. Exp. Med.* 197:1221–7.
- Pirozzi G, et al. (1997) Identification of novel human WW domain-containing proteins by cloning of ligand targets. *J. Biol. Chem.* 272:14611–6.
- Thomas RM, et al. (2004) C-terminal Src kinase controls acute inflammation and granulocyte adhesion. *Immunity.* 20:181–91.
- Ingle E. (2009) Csk-binding protein can regulate Lyn signals controlling cell morphology. *Int. J. Biochem. Cell. Biol.* 41:1332–43.
- Lee HH, et al. (2010) Src-dependent phosphorylation of ROCK participates in regulation of focal adhesion dynamics. *J. Cell Sci.* 123:3368–77.
- Lee HS, et al. (2007) Src tyrosine kinases mediate activations of NF-kappaB and integrin signal during lipopolysaccharide-induced acute lung injury. *J. Immunol.* 179:7001–11.
- Slater SJ, Seiz JL, Stagliano BA, Stubbs CD. (2001) Interaction of protein kinase C isoforms with Rho GTPases. *Biochemistry.* 40:4437–45.
- Fang X, et al. (2000) Phosphorylation and inactivation of glycogen synthase kinase 3 by protein kinase A. *Proc. Natl. Acad. Sci. U. S. A.* 97:11960–5.
- Rosendahl A, et al. (2002) Activation of bone morphogenetic protein/Smad signaling in bronchial epithelial cells during airway inflammation. *Am. J. Respir. Cell Mol. Biol.* 27:160–9.
- Newman JH, et al. (2009) Mutation in the gene for bone morphogenetic protein receptor II as a cause of primary pulmonary hypertension in a large kindred. *N. Engl. J. Med.* 345:319–24.
- Liang KC, et al. (2007) Interleukin-1beta induces MMP-9 expression via p42/p44 MAPK, p38 MAPK, JNK, and nuclear factor-kappaB signaling pathways in human tracheal smooth muscle cells. *J. Cell. Physiol.* 211:759–70.
- Wang C-C, et al. (2005) Involvement of p42/p44 MAPK, p38 MAPK, JNK, and NF-kappaB in IL-1beta-induced VCAM-1 expression in human tracheal smooth muscle cells. *Am. J. Lung Cell. Mol. Physiol.* 288: L227–37.
- van den Blink B, et al. (2001) Human endotoxemia activates p38 MAP kinase and p42/44 MAP kinase, but not c-Jun N-terminal kinase. *Mol. Med.* 7:755–60.
- Jope R, Yuskaitis C, Beurel E. (2007) Glycogen synthase kinase-3 (GSK3): inflammation, diseases, and therapeutics. *Neurochem. Res.* 32:577–595.
- Zhang P, Katz J, Michalek SM. (2009) Glycogen synthase kinase-3beta (GSK3beta) inhibition suppresses the inflammatory response to Francisella infection and protects against tularemia in mice. *Mol. Immunol.* 46:677–87.
- Beurel E, Michalek SM, Jope RS. (2009) Innate and adaptive immune responses regulated by glycogen synthase kinase-3 (GSK3). *Trends Immunol.* 31:24–31.
- Severgnini M, et al. (2004) Activation of the STAT pathway in acute lung injury. *Am. J. Lung Cell. Mol. Physiol.* 286:L1282–92.
- Lee YG, et al. (2008) Src kinase-targeted anti-inflammatory activity of davallialactone from *Inonotus vermicularis* in lipopolysaccharide-activated RAW264.7 cells. *Br. J. Pharmacol.* 154:852–63.
- Page TH, Smolinska M, Gillespie J, Urbaniak AM, Foxwell BM. (2009) Tyrosine kinases and inflammatory signalling. *Curr. Mol. Med.* 9:69–85.